Nature Environment and Pollution Technology
An International Quarterly Scientific Journal

p-ISSN: 0972-6268
(Print copies up to 2016)
e-ISSN: 2395-3454

Vol. 24 | No. S1 | pp. 339-353 | 2025

Original Research Paper

https://doi.org/10.46488/NEPT.2025.v24iS1.026

Open Access Journal

Efficient Removal of Congo Red Dye Using Activated Carbon Derived from Mixed Fish Scales Waste: Isotherm, Kinetics and Thermodynamics Studies

Vevosa Nakro[1], Ketiyala Ao[1], Tsenbeni N. Lotha[1], Imkongyanger Ao[1], Lemzila Rudithongru[1], Chubaakum Pongener[1], Merangmenla Aier[2], Aola Supong[3] and Latonglila Jamir[1]†

[1]Department of Environmental Science, Nagaland University, Lumami Campus-798627, Nagaland, India
[2]Department of Chemistry, National Institute of Technology, Nagaland, Chumoukedima-797103, Nagaland, India
[3]Department of Chemistry, Sao Chang College, Nagaland, India
†Corresponding author: Latonglila Jamir; latongli.jamir@gmail.com

Nat. Env. & Poll. Tech.
Website: www.neptjournal.com

Received: 20-04-2024
Revised: 04-06-2024
Accepted: 19-06-2024

Key Words:
Activated carbon
Congo red dye removal
Regeneration
Mixed fish scales

ABSTRACT

The discharge of large quantities of organic dyes into the environment causes significant harm to humans and the environment. Thus, there is an urgent need to develop cost-effective adsorbents for removing these dyes. In the present study, the synthesis of activated carbon (AC) derived from mixed fish scale waste using KOH activation was investigated for Congo red (CR) dye removal. The finding shows that the obtained biocarbon has a fixed carbon of 42.9% with a crystallinity index of 15.01%. N_2 adsorption-desorption isotherm was found to be type IV, signifying mesoporous structure with a surface area and total pore volume of 150.049 $m^2\ g^{-1}$ and 0.119 $cm^3.g^{-1}$. Batch adsorption was carried out by various adsorbent doses, initial concentration, contact time, and pH to comprehend the effect of operating parameters on its removal efficacy. The isotherm studies fitted well for Freundlich with an R^2 of 0.99%. Adsorption kinetics was best fitted by the pseudo-second-order model and thermodynamic studies revealed the adsorption process to be exothermic and spontaneous. The efficiency of AC was also studied by an amount of sorption and desorption cycles which showed its potential for reusability up to the sixth cycle. Thus, the findings suggest that activated carbon derived from mixed fish scale waste is a promising adsorbent for removing Congo red dye from aqueous solutions.

INTRODUCTION

Dyes present in aqueous solutions are highly visible even at low concentrations and pose significant health and environmental risks due to their harmful effects on humans and ecosystems. It can be classed as cationic, anionic, or non-ionic depending on its properties and structure(Agarwal et al. 2023). The sources include industries like food, printing, textiles, leather, pulp/paper mills, plastics, cosmetics, and pharmaceuticals (Jasińska et al. 2019), which can lead to the creation of a hypoxic environment in water. Approximately 10,000 diverse dyes and pigments, totaling 700,000 tons, are used in industries each year out of which 10-15% end up in water bodies (Bhatia et al. 2017). Among them, congo red (CR) is a widely used anionic azo dye in textile and paper dyeing (Fig. 1) (Lade et al. 2015). Known for its six aromatic rings, this anionic diazo dye is highly toxic and mutagenic, also resistant to natural degradation. It can irritate the skin and gastrointestinal tract, and it decomposes into carcinogens, posing significant risks to both human health and environmental safety (Li et al. 2023). Additionally, it is often illicitly added to meat and meat products as a coloring agent due to its low cost, high stability, and excellent dyeing properties (Wang et al. 2023). According to Jain and co-workers (Jain & Sikarwar 2014), it is stable in the atmosphere and may also be used as an indicator. It can also be used in gamma-ray dosimeters since its color diminishes with radiation strength(Rajhans et al. 2020). Prolonged dye contact with the skin or eyes might cause severe irritability due to the dye's extreme toxicity and when consumed it can cause nausea, vomiting, and diarrhea (Lade et al. 2015). CR dye displays different types of toxic effects including skin-related, environmental, microbial, yeast, bacterial, algal, and protozoan toxicity that exhibits genotoxic and cytotoxic effects with the ability to produce genetic alterations and cancer (Rajhans et al. 2020).

Over the decades, wastewater has been treated using diverse approaches like photocatalysis(Jorfi et al. 2016, Khan et al. 2023b), ultrafiltration (Hoslett et al. 2018, Yin et al. 2019), electrochemical processes (Islam et al. 2023), adsorption (Ukanwa et al. 2019, Burchacka et al. 2021), etc.

due to its effectiveness and cost efficiency, the adsorption technique is commonly employed methods for removing dyes from wastewater. AC branded by its significant surface area, high adsorption capacity, and cost-effectiveness, is a preferred choice for removing pollutants from aqueous solutions (Prajapati & Mondal 2020, Lotha et al. 2024, Sh et al. 2024).

Following this, a range of plant sources have been used to synthesize activated carbon, including rice husk rice (Feuzer-Matos et al. 2021), pistachio shells (Nejadshafiee & Islami 2019) coconut shells (Kosheleva et al. 2019, Muzarpar et al. 2020, Prajapati & Mondal 2020), bamboo (Lou et al. 2022), agricultural residues (Adamu & Adie 2020), bagasse (Van Tran et al. 2017), olive stone (Limousy et al. 2017), Manihot esculenta (Pongener et al. 2018), palm shell (Muzarpar et al. 2020), neem husk (Pathak 2023), apple peels (Jedynak & Charmas 2024), banana peels (Shukla et al. 2020), pine cone (Bhomick et al. 2018), almond shells (Boulika et al. 2023), litchi shell (Zhang et al. 2014) and *Tithonia diversifolia* (Supong et al. 2019a), etc. On the contrary, AC derived from animal biomass has not received significant attention in the existing literature with only a few reports which include cow manure (Park et al. 2022), pig bone (Liu et al. 2020), buffalo bone (Khan et al. 2023a), chicken bones (Khan et al. 2023a), donkey and horse bones (Jerome Sunday 2019), egg shells (Ahmad et al. 2020a), animal hair (Liu et al. 2013a), snail shell (Adiotomre 2015), sheep and goat dung (Kandasamy et al. 2023), etc. as it is known to hold many advantages, especially regarding its efficiency in removing pollutants and cost-effectiveness (Sh et al. 2024).

Fish scales, among other animal biowaste, have been found to have high percentages of carbon content and an insignificant amount of ash content, making them a promising source for AC synthesis (Stevens & Batlokwa 2017, Côrtes et al. 2019, Kodali et al. 2022). The removal of CR has been achieved by AC synthesized from shrimp shells which possess an adsorption capacity of 288.2 $mg.g^{-1}$ (Zhou et al. 2018). Similarly, bael shells-based AC showed high adsorption capacity of 98.03 $mg.g^{-1}$ towards the removal of CR (Ahmad & Kumar 2010). Hence, this study aims to utilize mixed fish scales (mFS) waste for AC production in CR dye removal. Various analytical techniques were used to characterize the synthesized adsorbent. Additionally, the effects of adsorbent dose, CR concentration, contact time, and pH on its adsorption were thoroughly investigated (Manjuladevi & Sri 2017, Mondal & Basu 2019). Furthermore, the isotherm, kinetics, and thermodynamics of the CR adsorption process on AC were examined and the potential reusability of the adsorbent was explored.

The unique aspect of using fish scales is their abundant availability, cost-effectiveness, and high carbon content, making them a sustainable and efficient raw material for activated carbon production. Although fish scales have been used before for this purpose, our study introduces a novel approach by utilizing mixed fish scale waste. This approach has the potential to improve adsorption capabilities, providing a practical solution for both waste management and dye removal. While previous research has investigated the use of AC derived from other biomass sources for CR removal, there is a gap in the literature regarding its application using waste mixed fish scales biomass.

MATERIALS AND METHODS

Materials

Mixed fish scales (mFS) were collected from the local fish market in Mokokchung town, Nagaland, India (26°19'38" N latitude and 94°31' 26" E longitude). Initially, the collected mFS were washed with distilled water, rinsed, and then dried in an oven at 120°C for 48 h. CR dye used in the current work was procured from Thermo ScientificTM. KOH, HCl, and NaOH were acquired from HI MEDIA (India) while HNO_3, KNO_3, and H_2SO_4 were obtained from Sigma Aldric.

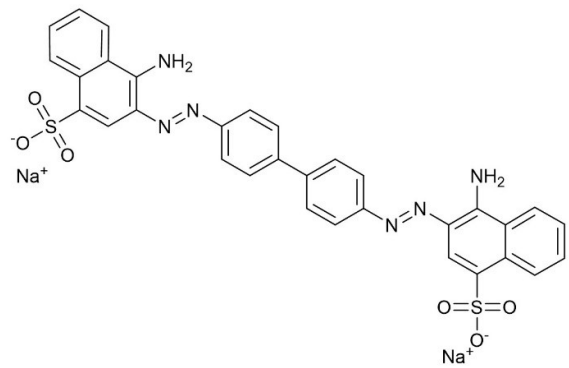

Fig. 1: Chemical structure of Congo Red.

Preparation of mixed fish scales (mFS) activated carbon: The collected biomass i.e. mixed fish scales were pyrolyzed at 500 °C for 1 h in a muffle furnace. After carbonization, the sample was ground and sieved into a fine powder using 212µ mesh and then subjected to KOH activation. Here, KOH was chosen as an activating agent because it creates a highly porous structure with a large surface area, allowing the AC to remove dye more efficiently from aqueous solutions. The resulting powder was labeled as mixed fish scales unactivated carbon (mFSUC). For activation, 200 mL of 10% KOH solution was mixed with 10 g of mFSUC. It was then stirred at 24°C for 3 h before drying in an oven for 30 h at 130°C. Subsequently, the dried sample was pyrolyzed at 700ºC for 3 h. The sample was subsequently rinsed with 0.1 M HCl and deionized water to achieve a neutral pH. The prepared AC is further subjected to oven drying at 105°C, labeled as mixed fish scales activated carbon (mFSAC) for further analysis. The scheme of mFSAC production is depicted in Fig. 2.

Carbon yield % is represented using the equation below.

$$\text{Yield } \% = \frac{W_1}{W_2} \times 100 \quad \ldots(1)$$

where W_1 = AC final weight; W_2 = dried raw biomass initial weight (mixed fish scales).

Adsorbate preparation: A concentration of 1000 mg.L^{-1} stock solution of CR dye was prepared with an addition of 0.5 g dye to 500 mL of de-ionized water. This stock solution was then used as the base for creating various concentrations at a range of 10 to 100 mg.L^{-1}. Throughout the study, chemicals were utilized without additional purification, and all experiments were conducted using de-ionized water.

Characterization of mFSAC: Proximate analysis of the prepared AC was conducted following the guidelines provided by the American Society for Testing and Materials (Standard A.S.T.M. 1999, Mukherjee et al. 2011), whereas ultimate analysis was conducted by CHNS elemental analyzer (Model: EA30000, Eurovector, Italy). The measurement for determining the iodine number followed the procedure specified by ASTM (American Society for Testing and Materials) D4607-94(2006) (ASTM 2006). Brunauer–Emmett–Teller (BET) surface area was also analyzed by (Smart instrument, SS93/02). The dried sample of AC was applied as a thin layer onto carbon conducting tape and subsequently gold coated. The microstructure and morphology of the prepared mFSAC were examined using a Scanning Electron Microscope (SEM) at an accelerating voltage of 3 kV (Model: JSM-6360, JEOL). The prepared AC was then characterized using a Fourier Transform Infrared (FTIR) spectrometer (Model: Spectrum Two, made: PerkinElmer, USA) to analyze the surface functional groups and XRD analysis was performed (Model: ULTIMA IV, Rigaku, Japan) using CuKα radiation, scanning at a rate of °0.2 per minute. X-ray photoelectron spectroscopy (XPS) for the sample was also examined (Model: OHI 5000 VersaProbe 111, USA), whereas the zero-point charge of the AC was determined through a batch equilibrium test (Babić et al. 1999).

Adsorption experiments: The batch method was performed to study the CR dye adsorption from the aqueous solution. Each experiment was conducted in an Erlenmeyer flask with an initial CR concentration shaken at 160 rpm in a rotary shaker for a fixed time. The parameters considered for investigating the CR dye removal were: Adsorbent dose (0.1-0.5 g.L^{-1}), pH (3-10), concentration (10-100 mg.L^{-1}), contact time (10-100 min) and temperature (298-328 K). The filtrate of CR dye was measured at 497 nm using a UV-Vis Spectrophotometer (lambda 35, PerkinElmer). Three separate sets of adsorption tests were conducted. Removal Percentage (%) and adsorption capacity were calculated using the equation below.

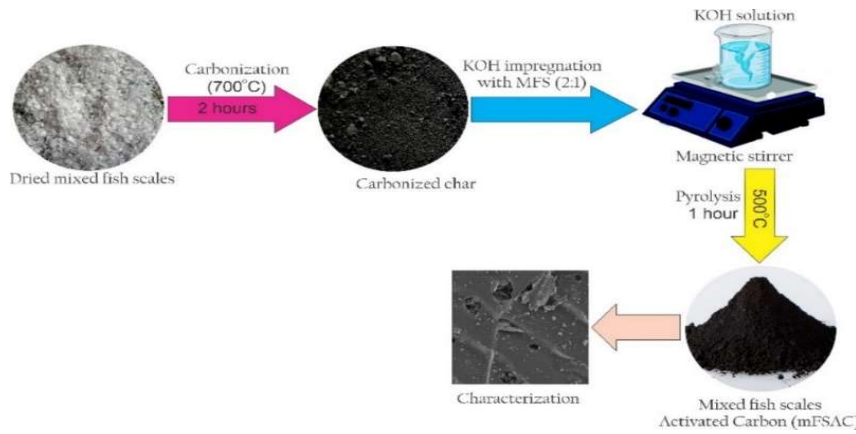

Fig. 2: Graphic illustration of mFSAC preparation.

$$\%\text{Removal of CR dye} = \frac{C_o - C_e}{C_o} \times 100 \quad \ldots(2)$$

$$q_e = \frac{(Co - Ce)}{M} \times V \quad \ldots(3)$$

Adsorption isotherms and kinetic experiments were investigated to comprehend the pollutant-adsorbent interaction (Belaib & Meniai 2016). The total quantity of CR retained by the AC was determined at various time intervals using the equation,

$$q_t = \frac{Co - Ct}{m} \times V \quad \ldots(4)$$

Here, C_o and C_e = initial and final concentrations, V = volume of CR solution; M = adsorbent mass, qt = amount of dye adsorbed, t = time taken, Ct = dye concentration at time t.

RESULTS AND DISCUSSION

Characterization of Prepared mFSAC

Physico-chemical properties of mFSAC are given in Table 1. The outcomes of the ultimate analysis are: carbon (C) 22.84%, hydrogen (H) 0.994%, nitrogen (N) 2.25%, and sulfur (S) 0.55%. The N_2 adsorption-desorption isotherm initiates the sample to be of type IV, indicating a mesoporous structure with a surface area of 150.049 $m^2.g^{-1}$ and a pore volume of 0.119 $cm^3.g^{-1}$. The values attained are in line with the synthesized AC's porosity and adsorptive properties. The prepared AC's elemental analysis revealed a much greater carbon content of 57.83% and a significantly lower ash level. The pHzpc, which correlates to the adsorbent's charge on its surface, was found to be 7.64 indicating that the carbon surface will be predominantly negative or positively charged respectively at a pH below or above 7.64 (Liu et al. 2013b, Habeeb et al. 2017).

Table 1: Different physio-chemical properties of mFSAC.

Proximate analysis (wt%)		Ultimate analysis: CHNS (wt%)	
Moisture	12.5%	C	22.84
Volatile	29.8 %	H	0.994
Ash	14.8 %	N	2.25
Fixed carbon	42.9%	S	0.055
Iodine number	210.67 $mg.g^{-1}$	BET surface area	150.049 $m^2.g^{-1}$
pH_{ZPC}	pH=7.64	Pore size	0.119 $cm^3.g^{-1}$

Scanning electron microscopy (SEM) analysis offers valuable data on the surface morphology of the synthesized mFSAC. The micrograph of the AC revealed an uneven surface with variable-sized pores and shapes dispersed throughout the surface (Fig. 3a). This could be owing to the interaction of KOH with the mFSAC, which results in the expansion of pores as a consequence of the elimination of volatile chemicals throughout the activation process (Supong et al. 2020, 2022). After the dye adsorption on the AC (Fig. 3b), SEM analysis can offer valuable insights into the alterations in the shape and structure of the material. The surface of the mFSAC post-dye adsorption appears rougher and more defined compared to the surface of AC before adsorption. This roughness is attributed to the attachment of CR dye molecules to the AC surface, leading to the formation of a complex three-dimensional network of dye molecules.

The FT-IR analysis was used to determine the existing functional groups as depicted in Fig.4. For mFSAC, at a wavelength of 3436 cm^{-1}, the adsorption band is attributed to the (O-H) hydroxyl group whereas the band at 2908 cm^{-1} may be ascribed to the stretching vibrations of the C-H bonds in alkanes and alkyl groups (Jiang et al. 2021). The vibrational modes of C=N bonds are also associated with

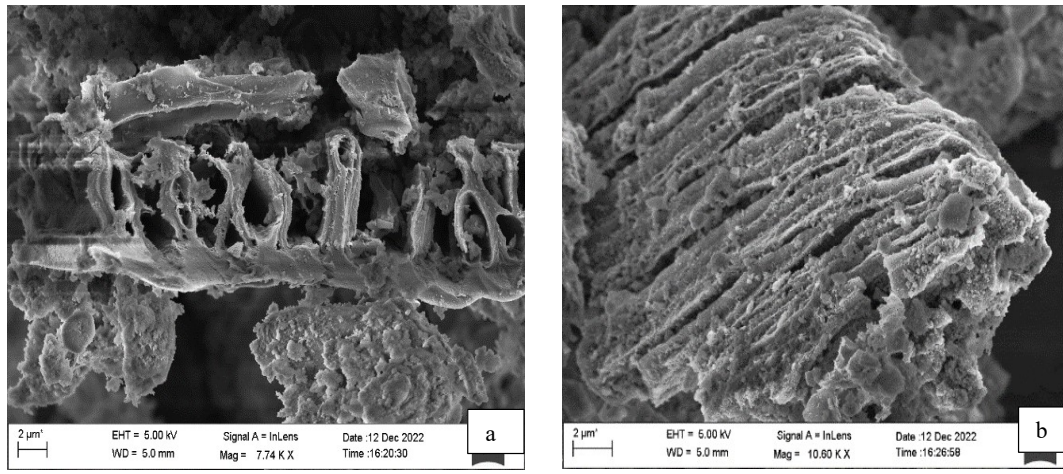

Fig. 3: SEM Micrograph of mFSAC (a) before, and (b) after adsorption.

bands at 1637 cm^{-1} and 2264 cm^{-1} (Bal Altuntaş et al. 2020). Furthermore, the existence of ether and ester functional groups which produce asymmetric stretching can be seen at wavelength 1208.66 cm^{-1} and 1020 cm^{-1} respectively (Alau et al. 2010). The prominent stretching vibrations of C–O, bending vibration of -OH groups, and C–H bonds result in IR peaks between 400 cm^{-1} and 800 cm^{-1} (Bhomick et al. 2018, Supong et al. 2019b). mFSUC at wavelength 3701 cm^{-1} attributes to the stretching vibration of the O-H (hydroxyl) groups. This can be indicative of free O-H groups, which are not hydrogen-bonded whereas the band at 1539 cm^{-1} is typically associated with the stretching vibrations of C=C bonds in aromatic rings or the bending vibrations of N-H bonds in amines. The absorption band at 1025 cm^{-1} is also commonly associated with the stretching vibrations of C-O bonds. After dye adsorption on the mFSAC, the band at 3733 cm^{-1} is typically attributed to the stretching vibration of free O-H groups whereas the absorption band at 1527 cm^{-1} is typically associated with the N-H bending vibration in amines or amides. It could also correspond to the aromatic C=C stretching vibrations.

XRD analysis was conducted on the prepared mFSAC with 2θ scan from 10° to 90°. The main peaks were found at 2θ = 26.24°, 32.15°, 39.8°, 49.0°, 58.86°, 64.33°, 76.0° and 88.10°, conforming to the d spacing of 0.34, 0.278, 0.225, 0.185, 0.145, 0.156, 0.125 and 0.12 nm respectively. The peaks about at 2θ = 26.24° and 32.15° indicate hydroxyapatite(Al-Malack & Basaleh 2016, Muthukumaran et al. 2016) and a peak at 2θ = 49.0° represents CaCO3 (Luo et al. 2020). Several peaks are in agreement with the reported peaks at 25.8°, 31.8°, 39.6°, and 49.3°, which resemble d spacings of 0.345, 0.281, 0.227, and 0.184 nm (Torres et al. 2008). The XRD profile of the mFSAC (Ratio 2:1) is depicted in Fig 5. The crystallite size of mFSAC is 4.2 nm and the degree of crystallinity was observed as 15.01% following the equation below,

$$D = \frac{k\lambda}{\beta \cos\theta} \quad \ldots(5)$$

$$\text{Crystallinity} = \frac{\text{Area of crystalline peak}}{\text{The overall area of peaks (crystalline+amorphous)}} \times 100 \quad \ldots(6)$$

The electron dispersive X-ray spectroscopy (EDX) analysis of the element percentage composition of mFSAC (Ratio 2:1) at 700 °C is shown in Fig. 6. The study revealed that the main components in its chemical structure were carbon (C) at 57.83% and oxygen (O) at 23.04% (Habeeb et al. 2017). Additionally, small amounts of Al, P, S, Ca, Br, Sb, and Pt were also detected.

The surface chemical composition of mFSAC using X-ray Photoelectron Spectroscopy (XPS) was analyzed. The wide scan spectra illustrating the chemical composition of mFSAC are presented in [Fig. 7 (a-c)]. The study indicated that carbon and oxygen were the most abundant elements. Specifically, carbon was observed at 284 eV and oxygen at 531 eV as the primary components. Further examination of the XPS spectrum at the Cls spectra with a binding energy of 284 eV revealed the presence of C-H or C-C groups, characteristic of graphitic carbon, and C-O groups, indicative of hydroxyl or ester functionalities. The major peaks in the O1s XPS spectra, with a binding energy of approximately 531 eV, corresponded to C-O carbonyl groups (Liu et al. 2020, An et al. 2022). The research offers valuable insights

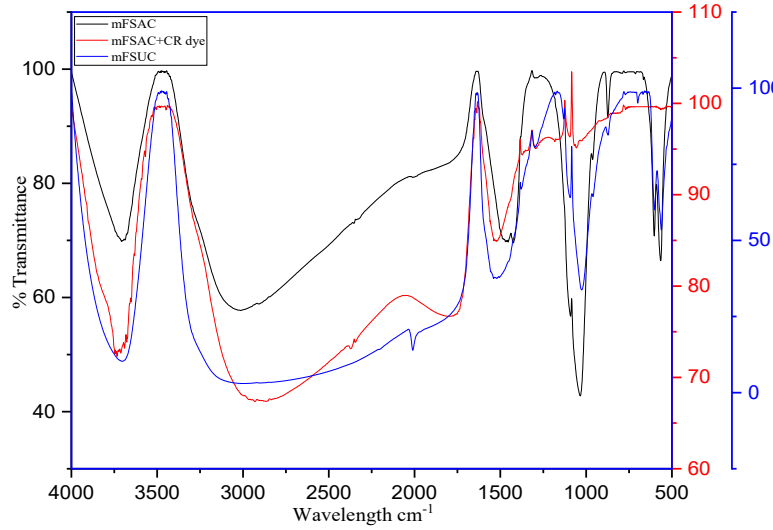

Fig. 4: FT-IR spectrum of mFSAC, mFSAC + CR dye, mFSAC.

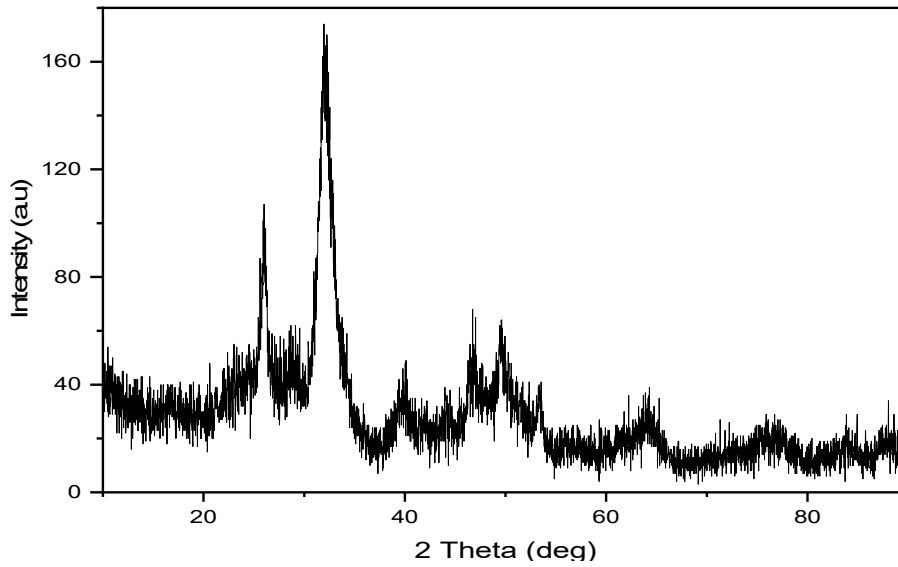

Fig. 5: XRD patterns of mFSAC.

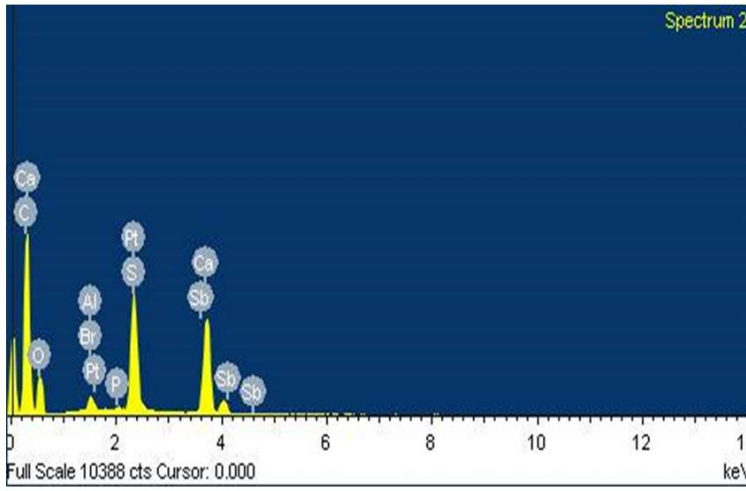

Element	Weight%	Atomic%
C K	57.83	71.46
O K	23.04	21.37
Al K	0.15	0.08
P K	0.18	0.09
S K	7.26	3.36
Ca K	8.78	3.25
Br L	1.14	0.21
Sb L	1.23	0.15
Pt M	0.40	0.03
Totals	100.00	

Fig. 6: EDX spectrum of mFSAC.

into the composition of mFSAC, specifically highlighting the presence of oxygen and carbon elements. Examination of the XPS spectrum indicated the existence of carbonyl groups and carbon bonds within the AC structure. These results are instrumental in characterizing AC and advancing our knowledge of its chemical composition, thereby facilitating the exploration of its potential applications.

Batch adsorption studies: Experimental variables like adsorbent dosage, initial concentration, contact time, pH, and temperature in the adsorption process were evaluated. Optimization of the equilibrium conditions was achieved through systematic variation of these parameters. At 25 °C, the CR concentrations were adjusted from 10-100 mg L^{-1}, AC dose: 0.1-0.5 g L^{-1}, and pH: 2-10 which was then shaken at 160 rpm. After the optimized conditions, the initial CR concentration, dosage, temperature, and contact time were 20 mg L^{-1}, 0.25 g L^{-1}, 25 °C, and 60 minutes, respectively. Mostly, significant removal of 99% was achieved at pH 4, making it an ideal pH for CR dye removal. The occurrence of OH^- ions in the solution, particularly at higher pH levels resulted in a decrease in adsorption capacities at elevated pH levels. These ions compete for available adsorption sites with the anionic dye (Beshkar et al. 2017, Alkurdi et al. 2019, Rajkumar et al. 2019).

For adsorbent efficiency, it is vital to study the effect of CR concentration and contact time. Various dye concentrations ranging from 10 to 100 mg L^{-1} were evaluated over a contact time of 0 to 100 minutes to understand the influence of

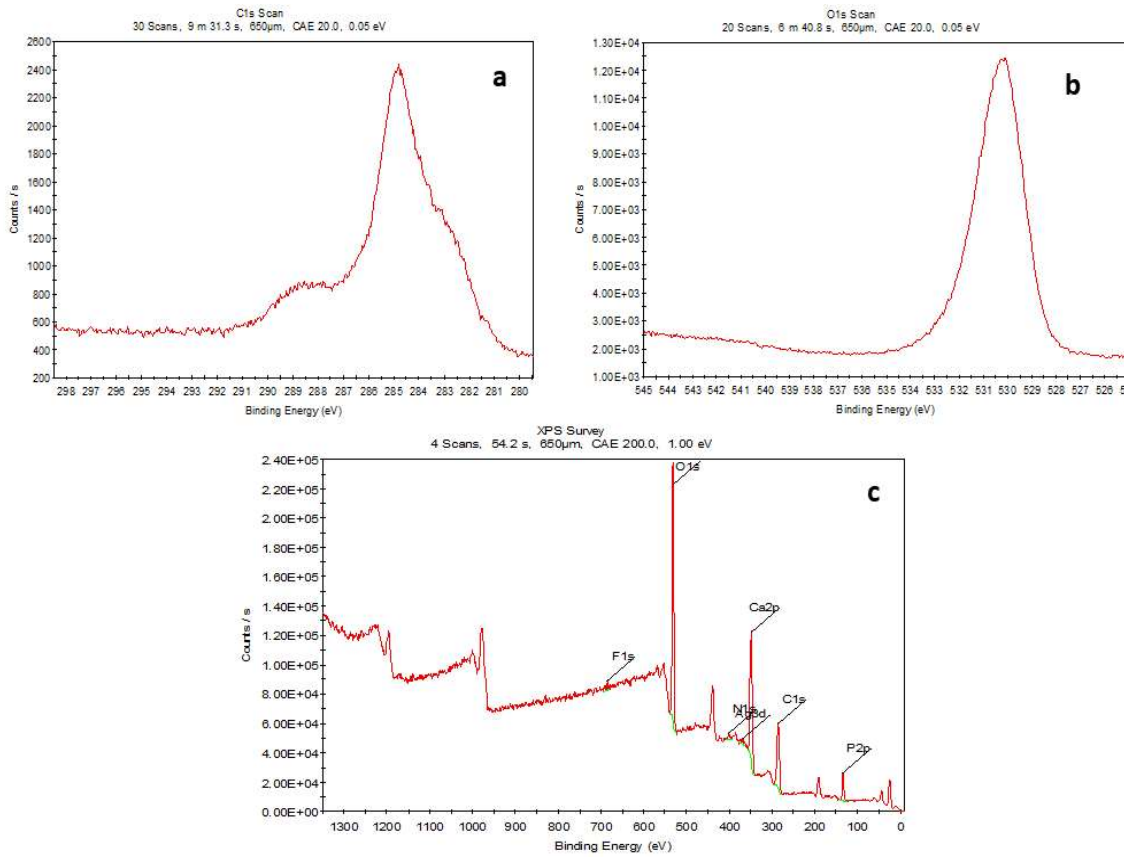

Fig. 7: XPS spectra of mFSAC; a) C1s, b) O1s, c) Overall wide scan.

the adsorption process. The results are shown in Fig 8(a) and (c), indicating that as dye concentration increased, the adsorption uptake also increased, reaching equilibrium at 60 minutes. Following an initial phase of rapid adsorption, the pace at which the adsorbent extracted dye from the solution decreased. This deceleration could be attributed to a decrease in the number of active sites accessible on the adsorbent's surface. Initially, numerous active sites may have been present for dye molecules to adhere to, resulting in rapid adsorption. However, as more dye molecules adhered to the surface, the number of active sites dwindled, leading to a deceleration in the adsorption rate (Ibrahim et al. 2016). Fig. 8(b) depicts the relationship between AC dosage and the removal percentage of CR at various concentrations. The removal efficiency of CR improved as the adsorbent dose increased for all CR concentrations until a dosage of 0.25 g of carbon was reached. This can be attributed to the large surface area of the mFSAC (Zhang et al. 2014, Dai et al. 2020). However, as the dosage exceeded 0.25 g, no significant changes were observed, indicating saturation of adsorbent binding sites with the dye molecules. Similar findings were found in a study on Ponceau 4R adsorption by Tilapia fish scales activated carbon treated with NaOH (Zhu et al. 2013). Subsequent readings were made keeping the optimal adsorbent dosage at 0.25 g.

pH levels from 2 to 10 were explored for CR dye adsorption utilizing mFSAC (Fig. 8d). The study shows that with an increase in pH from 2 to 10, the removal percentage and adsorption capacity of CR declined. This phenomenon can be ascribed to electrostatic interactions where pH levels lower than pH_{ZPC}, negatively charged CR molecules were attracted to the surface with a net positive charge. However, at pH levels exceeding the ZPC, the surface acquired a net negative charge, which repelled the negatively charged CR molecules, leading to decreased adsorption. Despite this trend, a high removal rate of 99% was observed at pH 4. The activated carbon's pHzpc was found to be close to neutral pH: 7.64, suggesting that both electrostatic and non-electrostatic interactions likely influenced CR dye adsorption. An increase in negatively charged -OH groups may compete with adsorption sites for negatively charged CR molecules at pH values greater than the pHZPC, which would reduce the percentage of dye removed (Bhomick et al. 2019). For instance, previous research has examined the adsorption of

Alizarin Red S using pine cone biocarbon and the adsorption of Ponceau 4R using Tilapia fish scales activated carbon (Zhu et al. 2013, Bhomick et al. 2018).

Adsorption isotherm studies: For equilibrium adsorption studies, the Langmuir, Freundlich, and Temkin adsorption models were analyzed with the experimental data such as the initial CR concentration: 20 $mg.L^{-1}$, dosage: 0.25 $g.L^{-1}$, temperature: 25°C and contact time: 60 minutes, respectively. One of many assumptions of the Langmuir isotherm is that adsorption happens on homogenous surfaces possessing equally energetic adsorption sites**.** Furthermore, equilibrium in the adsorbate-adsorbent system is reached when the adsorption of the adsorbate is confined to a single molecular layer, occurring at or before a relative pressure of unity is achieved (Shen et al. 2018). Our findings indicate that the Langmuir isotherm provides a q_{max} value of 19.58 $mg.g^{-1}$ with an $R^2 = 0.96$, suggesting a good fit. Additionally, the calculated separation factor, $R_L = 0.035$, indicates a favorable adsorption process (Giraldo & Moreno-Piraján 2014). The Freundlich isotherm analysis utilizes the heterogeneity factor, represented as nF, to determine if the adsorption process is linear (nF = 1), chemical (nF < 1), or physical (nF > 1). Our results indicating nF = 0.278 and 1/nF = 3.602, suggest the favorability of physical processes and cooperative adsorption (Idrees et al. 2018). High $R^2 = 0.99$, obtained when fitting the data to Freundlich isotherm confirms its appropriateness for our study. The preference for the Freundlich model in describing the adsorption process indicates adsorption on a heterogeneous surface with varying energies, allowing for multiple layers of adsorbate molecules. This aligns with AC's complex surface structure and diverse active sites. Additionally, the Freundlich model fits well for adsorbents with high capacities, like AC with its large surface area. Overall, the choice of the Freundlich model suggests it best captured the observed adsorption behavior, likely due to its good fit with the experimental data.

Temkin isotherm is designed to explicitly assess adsorbent-adsorbate interactions, yet its effectiveness in explaining CR dye adsorption onto mFSAC is reduced by $R^2 = 0.92$, particularly when associated with the Langmuir and

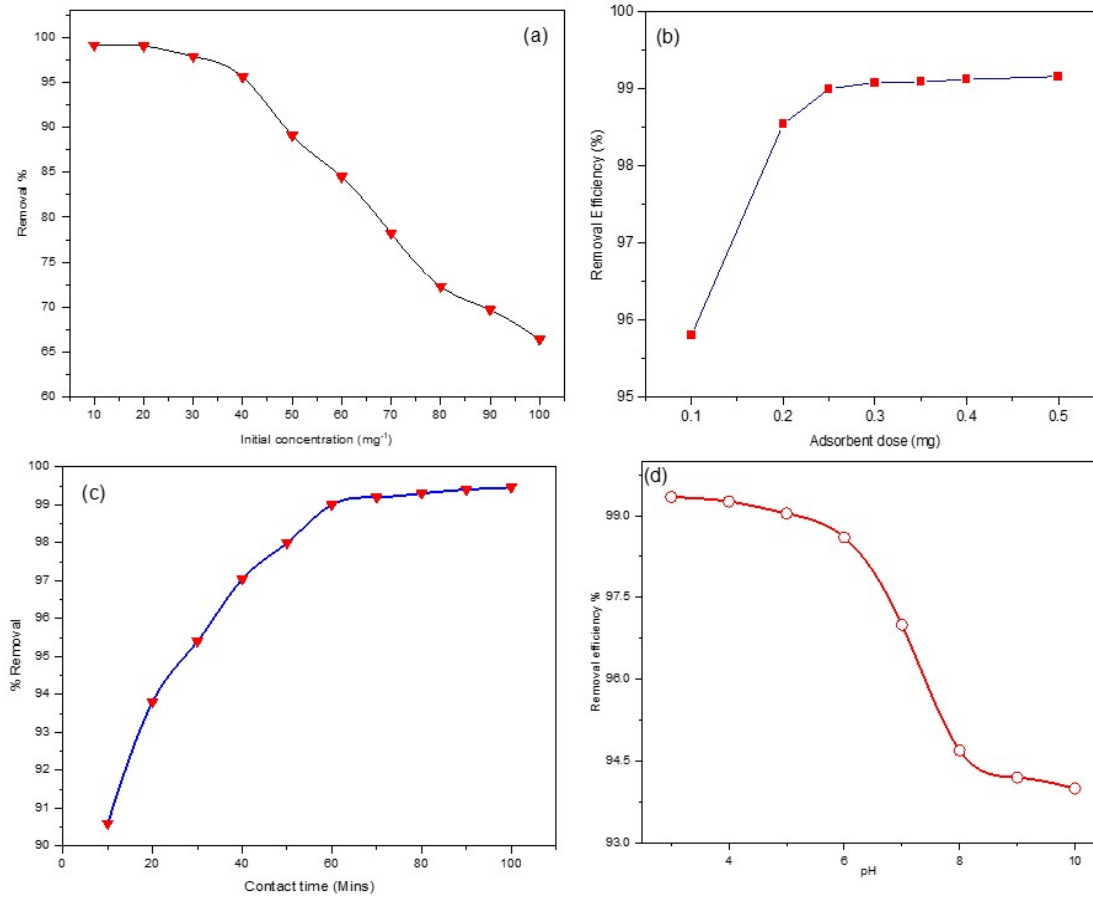

Fig. 8: Effect of mFSAC (a) Initial CR concentration (b) adsorbent dose (c) contact time and (d) pH.

Freundlich isotherms. The trial data indicates an exothermic process, as evidenced by a positive, BT = 8.56 which is associated with the heat of adsorption (Toor & Jin 2012, Ahmad et al. 2020b). Each adsorption isotherm model was confirmed using chi-square analysis. The Freundlich model exhibited the lowest $\chi 2$ values followed by the Langmuir and Temkin models using equation 7. This suggests that the Freundlich model more accurately describes the CR dye adsorption. Table 2 shows the values for each adsorption isotherm parameter.

$$\chi^2 = \sum \frac{\left(q_{e(exp)} - q_{e(cal)}\right)^2}{q_{e(cal)}} \quad \ldots(7)$$

Adsorption kinetics studies: Kinetic parameters are essential for developing and modeling the adsorption process, as well as understanding adsorption dynamics in relation to the order of rate constant. To know the experimental data for CR adsorption on mFSAC, models like pseudo-first-order (PFO), pseudo-second-order (PSO), intraparticle diffusion, and the Elovich model were analyzed. The earliest known equation that describes the adsorption capacity-based adsorption rate is the PFO (Bahgat et al. 2013). Whereas, the PSO is a chemisorption-based account of the adsorption process that contains valency forces and is explained by electron exchange between the sorbate and the solvent (Prajapati & Mondal 2020).

The PFO constant K_1 is derived from a linear plot of $\ln(q_e\text{-}q_t)$ vs time (Fig 9a). CR sorption on the mFSAC system was found to have a K_1 value of 0.00126/min, R^2 = 0.85, and an equilibrium sorption capacity $q_{e=}$ 1.958 mg g^{-1}. PFO is less advantageous than pseudo-second order due to its lower correlation coefficient and higher Sum of Squares Error (SSE) value (Table 3). The PSO model's correlation coefficient value of R^2 = 0.999 demonstrates the applicability of mFSAC (Fig 9b). In this context, the R^2 values have been determined to exhibit a stronger correlation, surpassing those of the PFO model by a significant margin. The results of the SSE study as well as $q_{e(cal)}$ and $q_{e(exp)}$ values further show that the PSO can more accurately and satisfactorily define the adsorption kinetics of CR onto mFSAC. Fig 9(c) depicts plots indicating the correlation between qt and $t_{1/2}$ for intraparticle diffusion. According to Demirbas and co-workers (Demirbas et al. 2008), the thickness of the boundary layer relies on the specific value of the intercept such that a thicker boundary layer results in a greater intercept value. The result indicates a different stage in the adsorption process, suggesting that intraparticle diffusion is the factor in the influence adsorption process. High R^2 = 0.958 indicates homogeneous pore structures with a strong linear relationship between solute uptake and the square root of time throughout the adsorption process (Adane et al. 2015). The Elovich model signifies that the rate of adsorption decreases over time and considers diffusion as the rate-determining phase (Grassi et al. 2019, Al-Harby et al. 2022). The outcomes are illustrated through a plot of qt against ln(t) resulting in a correlation coefficient R^2 = 0.926.

Thermodynamic studies: The assessment of thermodynamic parameters is a crucial and essential aspect of research on sorption processes which offer insights into whether the mechanism is predominantly influenced by chemical or physical interactions. The temperature range covered by the thermodynamic analysis of CR adsorption was 298 K to 328 K. The thermodynamic parameters can be calculated by using the equation below.

$$\ln K_d = \frac{\Delta S^\circ}{R} - \frac{\Delta H^\circ}{RT} \quad \ldots(8)$$

$$K_d = \frac{q_e}{C_e} \quad \ldots(9)$$

Table 2: Isotherm parameters for CR dye adsorption.

Isotherm	Equations	Parameters	R^2	
Langmuir	$q_e = \frac{K_L C_e}{1 + \alpha_L C_e}; \frac{C_e}{q_e} = \frac{1}{K_L} - \frac{\alpha_L}{K_L} C_e$	$q_{max}\left(\frac{\alpha_L}{K_L}\right)$ = 19.58 $\frac{1}{nF}$ = 0.787 K_L = 0.961 R_L = 0.035	0.96	0.0034
Freundlich	$\mathrm{Log}\left(\frac{X}{M}\right) = \frac{1}{nF}(\log C_e) + \log K_F$	$\frac{1}{nF}$ = 3.602 K_L = 0.166 R_L = 0.231 K_F = 46.697	0.99	0.00031
Temkin	$q_e = \frac{RT}{B_T} \ln(A_T C_e)$	B_T = 8.56 A= 3.16	0.92	0.1801

Table 3: Kinetic parameters of CR dye adsorption on mFSAC.

Kinetics	Equations	Parameters	R^2
Pseudo-first order	$\log(q_e - qt_t) = \log q_e - \frac{k1}{2.303}t$	$q_{e(exp)}$ =1.958 k_1 = 0.00126 SSE= 5.16 MSE= 0.73	0.85
Pseudo-Second order	$\frac{t}{q_t} = \frac{1}{k_{2q_e^2}} + \frac{1}{q_e}t$	$q_{e(exp)}$ = 1.95 $q_{e(cal)}$ =1.97 k_2 =1.08 SSE=0.042 MSE= 0.007	0.99
Intraparticle diffusion	$q_t = k_b t^{1/2} + A$	k_b = 0.010 $q_{e(exp)}$ = 1.95 $A(mg\ g^{-1})$ = 1.864	0.95
Elovich	$q_t = \frac{1}{\beta}\ln(\alpha\beta t) + \frac{1}{\beta}\ln(t)$	a = 2.765 b = 3.278 SSE = 0.54 MSE = 0.18	0.92

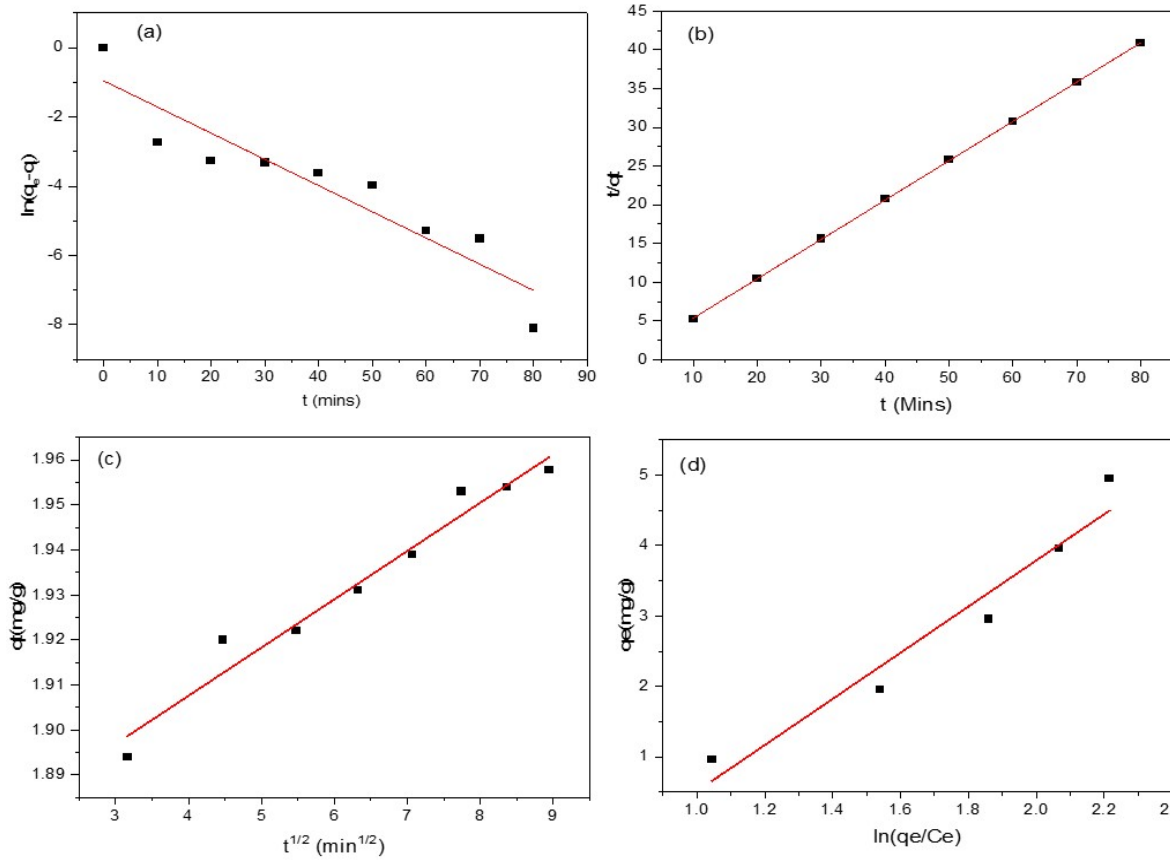

Fig. 9: (a) PFO (b) PSO (c) Intraparticle diffusion and (d) Elovich model.

$$\Delta G° = \Delta H° - T\Delta S° \quad \ldots(10)$$

Here, Ce =equilibrium concentration ($mg.L^{-1}$), R = 8.314 J mol/K, T = temperature, and qe = amount of dye adsorbed.

The study revealed ΔH values of -96.62 kJ mol^{-1} for CR adsorption, suggesting an exothermic behavior, and -ΔG values indicating the spontaneity and vitality of the adsorption process. Whereas - ΔS proposed that the sorption is enthalpy-driven throughout the adsorption phase and the rise in ΔG value with temperature up to 318 K highlighted its viability at lower temperatures (Table 4).

Comparative study of mFSAC and other absorbents: To evaluate the effectiveness of the mFSAC, a comparison was made with other adsorbents for the removal of CR. The study analyzed the removal % of mFSAC in comparison to various other adsorbents (Table 5). The results indicate that the AC derived from mixed fish scale wastes demonstrates a comparable adsorptive capacity to that of other adsorbents, highlighting its potential as an effective adsorbent for the removal of CR.

Regeneration studies: A regeneration study of mFSAC was performed by mixing 0.25 g of mFSAC with 20 mL of a 20 mg L^{-1} CR solution and allowing it to stir for 60 minutes. The saturated carbon was then subjected to desorption for 2 hours with the addition of 0.1 M NaOH solution. After desorption, the mFSAC was dehydrated at 110°C in an oven, filtered, and rinsed with distilled water. Fig 10 illustrates the removal % of mFSAC over six cycles. The results indicate a removal efficacy of 99% in the first cycle, decreasing to 72.68% by the sixth cycle. These findings suggest that the mFSAC can be reused multiple times and can be calculated using the following equation.

$$\text{Desorption efficiency (\%)} = \frac{q_{de}}{q_{ad}} \times 100 \quad \ldots(11)$$

CONCLUSİONS

This research explores potential applications for waste mixed fish scales (mFS) in generating activated carbon (AC) for adsorption purposes. Various physical properties of mFSAC were examined through approaches such as CHNS, BET, SEM, FTIR, XRD, EDX, and XPS. By employing batch mode operation, parameters like AC dose, initial CR dye concentration, contact time, pH, and temperature were explored. The Freundlich isotherm showed the strongest correlation (R^2 = 0.99) for dye adsorption, indicating a favorable adsorption process. The pseudo-second-order model suggests that the adsorption mechanism is chemisorption, implying a strong interaction between CR dye molecules and the AC surface. Thermodynamic analysis revealed that the adsorption process is temperature-dependent and exothermic. In conclusion, the study highlights the potential of using AC derived from discarded fish scales as an effective adsorbent for CR dye. This suggests an opportunity to repurpose waste fish scales into AC, which can address waste management issues and provide a valuable resource for various industries thus offering economic benefits, promoting environmental sustainability, and reducing reliance on non-renewable resources.

ACKNOWLEDGEMENT

Vevosa Nakro, Imkongyanger, Lemzila Rudithongru, and Ketiyala thank UGC, and Tsenbeni N. Lotha thank the Ministry of Tribal Affairs, GOI for a research fellowship.

Table 4: Thermodynamic parameters for CR dye onto mFSAC.

Adsorbent	ΔH° (kJ mol^{-1})	ΔS° (kJ mol^{-1})	ΔG° (kJ mol^{-1})			
			298K	308K	318K	328K
mFSAC	-96.62	-287.9	-11.40	-8.57	-3.19	-3.76

Table 5: Adsorption capacities of various adsorbents for CR removal.

Adsorbate	Adsorbent	Optimum parameters				Adsorption capacity ($mg.g^{-1}$)	Removal %	References
		Dosage	Initial concentration ($mg.L^{-1}$)	Contact time	pH			
Congo red	Fishbone	5g	150	60 min	2	666.67	96.3	(Parvin et al. 2021)
	Cuttlefish bone	50mg	50	60 min	2	69.9	94	(Yazid et al. 2021)
	Bael shell	50mg	50	180 min	3	98.03	92	(Ahmad and Kumar 2010)
	Trichoderma	-	50	24 h	6	81.82	88	(Argumedo-Delira et al. 2021)
	Coffee waste	4g	50	180 min	3	90.90	96.8	(Lafi et al. 2019)
	Azolla filiculoides	2g	200	-	6.2	243	95	(Sundararaman et al. 2021)
	Saw dust	1g	-	2.5 h	2	209	96.76	(Srinivas Kini et al. 2017)
	Raphanus sativus peels	2g	-	20 min	3	0.06	94	(Rehman et al. 2012)
	Grewiaasiatica leave	0.5g	-	30 min	7	0.56	95	
	Mixed Fish Scales	0.25g	20	60 min	4	19.58	99	This Study

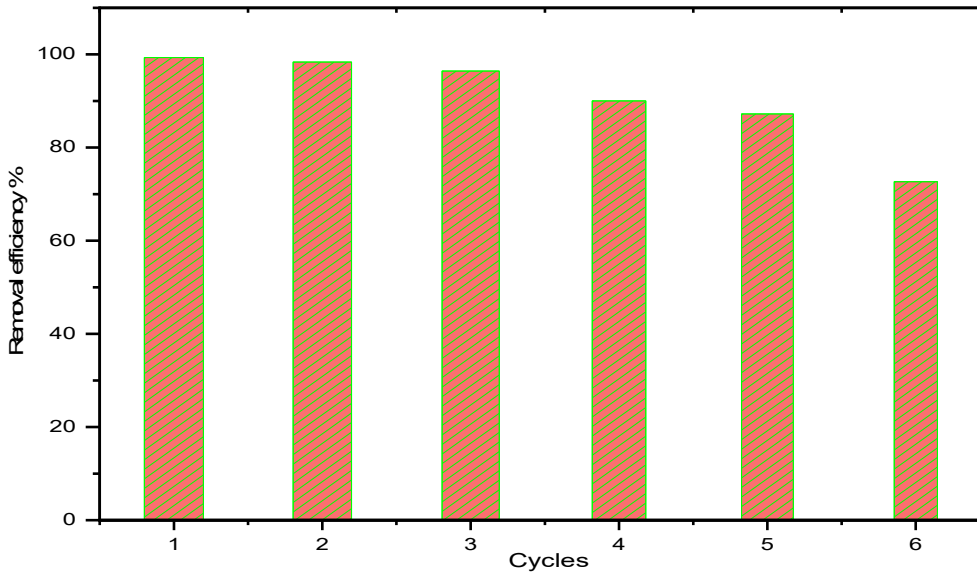

Fig. 10: Regeneration of mFSAC over six cycles.

REFERENCES

Adamu, A.D. and Adie, D.B., 2020. Assessment of lead adsorption onto rice husk activated carbon. *Nigerian Journal of Engineering*, 27(2), pp.2705–3954.

Adane, B., Siraj, K. and Meka, N., 2015. Kinetic, equilibrium and thermodynamic study of 2-chlorophenol adsorption onto Ricinus communis pericarp activated carbon from aqueous solutions. *Green Chemistry Letters and Reviews*, 8(3–4), pp.1–12. https://doi.org/10.1080/17518253.2015.1065348.

Adiotomre, K., 2015. Effectiveness of snail shell as an adsorbent for the treatment of waste water. *International Journal of Innovative Environmental Studies Research*, 3(3), pp.1–12.

Agarwal, S., Singh, A.P. and Mathur, S., 2023. Removal of COD and color from textile industrial wastewater using wheat straw activated carbon: an application of response surface and artificial neural network modeling. *Environmental Science and Pollution Research*, 30(14), pp.41073–41094. https://doi.org/10.1007/s11356-022-25066-2.

Ahmad, A., Jini, D., Aravind, M., Parvathiraja, C., Ali, R., Kiyani, M.Z. and Alothman, A., 2020a. A novel study on synthesis of egg shell based activated carbon for degradation of methylene blue via photocatalysis. *Arabian Journal of Chemistry*, 13(12), pp.8717–8722. https://doi.org/10.1016/j.arabjc.2020.10.002.

Ahmad, R. and Kumar, R., 2010. Adsorptive removal of congo red dye from aqueous solution using bael shell carbon. *Applied Surface Science*, 257(5), pp.1628–1633. https://doi.org/10.1016/j.apsusc.2010.08.111.

Ahmad, S., Kothari, R., Shankarayan, R. and Tyagi, V.V., 2020b. Temperature dependent morphological changes on algal growth and cell surface with dairy industry wastewater: an experimental investigation. *3 Biotech*, 10(1), pp.1–12. https://doi.org/10.1007/s13205-019-2008-x.

Alau, K.K., Gimba, C.E., Kagbu, J.A. and Nale, B.Y., 2010. Preparation of activated carbon from neem (Azadirachta indica) husk by chemical activation with H_3PO_4, KOH and $ZnCl_2$. *Arch. Appl. Sci. Res.*, *2*(5), pp.451-455.

Al-Harby, N.F., Albahly, E.F. and Mohamed, N.A., 2022. Synthesis and Characterization of novel uracil-modified chitosan as a promising adsorbent for efficient removal of congo red dye. *Polymers*, 14(2), p.271. https://doi.org/10.3390/polym14020271.

Al-Malack, M.H. and Basaleh, A.A., 2016. Adsorption of heavy metals using activated carbon produced from municipal organic solid waste. *Desalination and Water Treatment*, 57(02), pp.24519–24531. https://doi.org/10.1080/19443994.2016.1144536.

Alkurdi, S.S.A., Herath, I., Bundschuh, J., Al-Juboori, R.A., Vithanage, M. and Mohan, D., 2019. Biochar versus bone char for a sustainable inorganic arsenic mitigation in water: What needs to be done in future research? *Environment International*, 127(3), pp.52–69. https://doi.org/10.1016/j.envint.2019.03.012.

An, J., Nhung, N.T.H., Ding, Y., Chen, H., He, C., Wang, X. and Fujita, T., 2022. Chestnut shell-activated carbon mixed with pyrolytic snail shells for methylene blue adsorption. *Materials*, 15(22), pp.1–25. https://doi.org/10.3390/ma15228227.

Argumedo-Delira, R., Gómez-Martínez, M.J. and Uribe-Kaffure, R., 2021. Trichoderma biomass as an alternative for removal of congo red and malachite green industrial dyes. *Applied Sciences*, 11(1), pp.1–15. https://doi.org/10.3390/app11010448.

ASTM, D., 2006. 4607-94, Standard test method for determination of iodine number of activated carbon. *ASTM International: West Conshohocken, PA, USA*.

Babić, B.M., Milonjić, S.K., Polovina, M.J. and Kaludierović, B.V., 1999. Point of zero charge and intrinsic equilibrium constants of activated carbon cloth. *Carbon*, 37(3), pp.477–481. https://doi.org/10.1016/S0008-6223(98)00216-4.

Bahgat, M., Farghali, A.A., El Rouby, W., Khedr, M. and Mohassab-Ahmed, M.Y., 2013. Adsorption of methyl green dye onto multi-walled carbon nanotubes decorated with Ni nanoferrite. *Applied Nanoscience*, 3(3), pp.251–261. https://doi.org/10.1007/s13204-012-0127-3.

Bal Altuntaş, D., Nevruzoğlu, V., Dokumacı, M. and Cam, Ş., 2020. Synthesis and characterization of activated carbon produced from waste human hair mass using chemical activation. *Carbon Letters*, 30(3), pp.307–313. https://doi.org/10.1007/s42823-019-00099-9.

Belaib, F. and Meniai, A.-H., 2016. The removal of cationic dye (Methyl green) dye by adsorbant based Silica gel/Polymer. *Algerian Journal of Engineering Research*, pp.1–5.

Beshkar, F., Zinatloo-Ajabshir, S., Bagheri, S. and Salavati-Niasari, M., 2017. Novel preparation of highly photocatalytically active copper chromite nanostructured material via a simple hydrothermal route. *PLoS One*, 12(6), pp.17–18. https://doi.org/10.1371/journal.pone.0158549.

Bhatia, D., Sharma, N.R., Singh, J. and Kanwar, R.S., 2017. Biological

methods for textile dye removal from wastewater: A review. *Critical Reviews in Environmental Science and Technology*, 47(19), pp.1836–1876. https://doi.org/10.1080/10643389.2017.1393263.

Bhomick, P.C., Supong, A., Baruah, M., Pongener, C. and Sinha, D., 2018. Pine Cone biomass as an efficient precursor for the synthesis of activated biocarbon for adsorption of anionic dye from aqueous solution: Isotherm, kinetic, thermodynamic and regeneration studies. *Sustainable Chemistry and Pharmacy*, 10(June), pp.41–49. https://doi.org/10.1016/j.scp.2018.09.001.

Bhomick, P.C., Supong, A., Karmaker, R., Baruah, M., Pongener, C. and Sinha, D., 2019. Activated carbon synthesized from biomass material using single-step KOH activation for adsorption of fluoride: Experimental and theoretical investigation. *Korean Journal of Chemical Engineering*, 36(4), pp.551–562. https://doi.org/10.1007/s11814-019-0234-x.

Boulika, H., El Hajam, M., Hajji Nabih, M., Riffi Karim, I., Idrissi Kandri, N. and Zerouale, A., 2023. Definitive screening design applied to cationic & anionic adsorption dyes on Almond shells activated carbon: Isotherm, kinetic and thermodynamic studies. *Materials Today: Proceedings*, 72(8), pp.3336–3346. https://doi.org/10.1016/j.matpr.2022.07.358.

Burchacka, E., Pstrowska, K., Beran, E., Fałtynowicz, H., Chojnacka, K. and Kułazynski, M., 2021. Antibacterial agents adsorbed on active carbon: a new approach for S. aureus and E. coli pathogen elimination. *Pathogens*, 10(8), pp.1–15.

Côrtes, L.N., Druzian, S.P., Streit, A.F.M., Godinho, M., Perondi, D., Collazzo, G.C., Oliveira, M.L.S., Cadaval, T.R.S. and Dotto, G.L., 2019. Biochars from animal wastes as alternative materials to treat colored effluents containing basic red 9. *Journal of Environmental Chemical Engineering*, 7(6), pp.1–39. https://doi.org/10.1016/j.jece.2019.103446.

Dai, Y., Wang, W., Lu, L., Yan, L. and Yu, D., 2020. Utilization of biochar for the removal of nitrogen and phosphorus. *Journal of Cleaner Production*, 257(2), p.120573. https://doi.org/10.1016/j.jclepro.2020.120573.

Demirbas, E., Kobya, M. and Sulak, M.T., 2008. Adsorption kinetics of a basic dye from aqueous solutions onto apricot stone activated carbon. *Bioresource Technology*, 99(13), pp.5368–5373. https://doi.org/10.1016/j.biortech.2007.11.019.

Feuzer-Matos, A.J., Testolin, R.C., Cotelle, S., Sanches-Simões, E., Pimentel-Almeida, W., Niero, G., Walz, G.C., Ariente-Neto, R., Somensi, C.A. and Radetski, C.M., 2021. Degradation of recalcitrant textile azo-dyes by fenton-based process followed by biochar polishing. *Journal of Environmental Science and Health - Part A*, 56(9), pp.1019–1029. https://doi.org/10.1080/10934529.2021.1959774.

Giraldo, L. and Moreno-Piraján, J.C., 2014. Study of adsorption of phenol on activated carbons obtained from eggshells. *Journal of Analytical and Applied Pyrolysis*, 106(12), pp.41–47. https://doi.org/10.1016/j.jaap.2013.12.007.

Grassi, P., Reis, C., Drumm, F.C., Georgin, J., Tonato, D., Escudero, L.B., Kuhn, R., Jahn, S.L. and Dotto, G.L., 2019. Biosorption of crystal violet dye using inactive biomass of the fungus Diaporthe schini. *Water Science and Technology*, 79(4), pp.709–717. https://doi.org/10.2166/wst.2019.091.

Habeeb, O.A., Kanthasamy, R., Ali, G.A.M. and Yunus, R.M., 2017. Isothermal modelling based experimental study of dissolved hydrogen sulfide adsorption from waste water using eggshell based activated carbon. *Malaysian Journal of Analytical Sciences*, 21(2), pp.334–345. https://doi.org/10.17576/mjas-2017-2102-08.

Hoslett, J., Massara, T.M., Malamis, S., Ahmad, D., van den Boogaert, I., Katsou, E., Ahmad, B., Ghazal, H., Simons, S., Wrobel, L. and Jouhara, H., 2018. Surface water filtration using granular media and membranes: A review. *Science of the Total Environment*, 639(05), pp.1268–1282. https://doi.org/10.1016/j.scitotenv.2018.05.247.

Ibrahim, W.M., Hassan, A.F. and Azab, Y.A., 2016. Biosorption of toxic heavy metals from aqueous solution by Ulva lactuca activated activated carbon. *Egyptian Journal of Basic and Applied Sciences*, 3(3), pp.241–249. https://doi.org/10.1016/j.ejbas.2016.07.005.

Idrees, M., Batool, S., Kalsoom, T., Yasmeen, S., Kalsoom, A., Raina, S. and Kong, J., 2018. Animal manure-derived biochars produced via fast pyrolysis for the removal of divalent copper from aqueous media. *Journal of Environmental Management*, 213(2), pp.109–118. https://doi.org/10.1016/j.jenvman.2018.02.003.

Islam, M.M., Mohana, A.A., Rahman, M.A., Rahman, M., Naidu, R. and Rahman, M.M., 2023. A comprehensive review of the current progress of chromium removal methods from aqueous solution. *Toxics*, 11(3), pp.1–43. https://doi.org/10.3390/toxics11030252.

Jain, R. and Sikarwar, S., 2014. Adsorption and desorption studies of Congo red using low-cost adsorbent: activated de-oiled mustard. *Desalination and Water Treatment*, 52(37–39), pp.7400–7411. https://doi.org/10.1080/19443994.2013.837004.

Jasińska, A., Soboń, A., Góralczyk-Bińkowska, A. and Długoński, J., 2019. Analysis of decolorization potential of *Myrothecium roridum* in the light of its secretome and toxicological studies. *Environmental Science and Pollution Research*, 26(25), pp.26313–26323. https://doi.org/10.1007/s11356-019-05324-6.

Jedynak, K. and Charmas, B., 2024. Adsorption properties of biochars obtained by KOH activation. *Adsorption*, 30(2), pp.167–183. https://doi.org/10.1007/s10450-023-00399-7.

Jerome Sunday, N., 2019. Efficiency of animal (cow, donkey, chicken and horse) bones, in removal of hexavalent chromium from aqueous solution as a low cost adsorbent. *American Journal of Applied Chemistry*, 7(1), p.1. https://doi.org/10.11648/j.ajac.20190701.11.

Jiang, H., Guo, G., Chen, W. and Cui, Z., 2021. Reactive dyeing of synthetic fibers employing dyes containing a diazirine moiety. *Dyes and Pigments*, 194(1), p.109555. https://doi.org/10.1016/j.dyepig.2021.109555.

Jorfi, S., Barzegar, G., Ahmadi, M., Darvishi Cheshmeh Soltani, R., Alah Jafarzadeh Haghighifard, N., Takdastan, A., Saeedi, R. and Abtahi, M., 2016. Enhanced coagulation-photocatalytic treatment of Acid red 73 dye and real textile wastewater using UVA/synthesized MgO nanoparticles. *Journal of Environmental Management*, 177(07), pp.111–118. https://doi.org/10.1016/j.jenvman.2016.04.005.

Kandasamy, S., Madhusoodanan, N., Senthilkumar, P., Muneeswaran, V., Manickam, N. and Myneni, V.R., 2023. Adsorption of methylene blue dye by animal dung biomass–derived activated carbon: optimization, isotherms and kinetic studies. *Biomass Conversion and Biorefinery*, (8), pp.1–15. https://doi.org/10.1007/s13399-023-04710-y.

Khan, A.M., Usmani, M.A., Yasmeen, K., Ahmed, M.N., Obaid, M., Afshan Naz, S., Wajid, M., Chan, H. and Khan, A., 2023a. Conversion of waste animal bones to biofertilizer and adsorbent for wastewater treatment: An innovative approach to develop zero-waste technology.

Khan, Z.U.H., Gul, N.S., Sabahat, S., et al., 2023b. Removal of organic pollutants through hydroxyl radical-based advanced oxidation processes. *Ecotoxicology and Environmental Safety*, 267(10), p.115564. https://doi.org/10.1016/j.ecoenv.2023.115564.

Kodali, D., Hembrick-Holloman, V., Gunturu, D.R., Samuel, T., Jeelani, S. and Rangari, V.K., 2022. Influence of Fish Scale-Based Hydroxyapatite on Forcespun Polycaprolactone Fiber Scaffolds. *ACS Omega*, 7(10), pp.8323–8335. https://doi.org/10.1021/acsomega.1c05593.

Kosheleva, R.I., Mitropoulos, A.C. and Kyzas, G.Z., 2019. Synthesis of activated carbon from food waste. *Environmental Chemistry Letters*, 17(1), pp.429–438. https://doi.org/10.1007/s10311-018-0817-5.

Lade, H., Govindwar, S. and Paul, D., 2015. Mineralization and detoxification of the carcinogenic azo dye Congo red and real textile effluent by a polyurethane foam immobilized microbial consortium in an upflow column bioreactor. *International Journal of Environmental Research and Public Health*, 12(6), pp.6894–6918. https://doi.org/10.3390/ijerph120606894.

Lafi, R., Montasser, I. and Hafiane, A., 2019. Adsorption of congo

red dye from aqueous solutions by prepared activated carbon with oxygen-containing functional groups and its regeneration. *Adsorption Science & Technology*, 37(1–2), pp.160–181. https://doi.org/10.1177/0263617418819227.

Li, H., Fei, J., Chen, S., Jones, K.C., Li, S., Chen, W. and Liang, Y., 2023. An easily-synthesized low carbon ionic liquid functionalized metal-organic framework composite material to remove Congo red from water. *Water Cycle*, 4(5), pp.127–134. https://doi.org/10.1016/j.watcyc.2023.05.004.

Limousy, L., Ghouma, I., Ouederni, A. and Jeguirim, M., 2017. Amoxicillin removal from aqueous solution using activated carbon prepared by chemical activation of olive stone. *Environmental Science and Pollution Research*, pp.9993–10004. https://doi.org/10.1007/s11356-016-7404-8.

Liu, H., Ning, W., Cheng, P., Zhang, J., Wang, Y. and Zhang, C., 2013a. Evaluation of animal hairs-based activated carbon for sorption of norfloxacin and acetaminophen by comparing with cattail fiber-based activated carbon. *Journal of Analytical and Applied Pyrolysis*, 5(101), pp.156–165.

Liu, H., Ning, W., Cheng, P., Zhang, J., Wang, Y. and Zhang, C., 2013b. Evaluation of animal hairs-based activated carbon for sorption of norfloxacin and acetaminophen by comparing with cattail fiber-based activated carbon. *Journal of Analytical and Applied Pyrolysis*, 101, pp.156–165. https://doi.org/10.1016/j.jaap.2013.01.016.

Liu, Y., Xu, J., Cao, Z., Fu, R., Zhou, C., Wang, Z. and Xu, X., 2020. Adsorption behavior and mechanism of Pb(II) and complex Cu(II) species by biowaste-derived char with amino functionalization. *Journal of Colloid and Interface Science*, 559(10), pp.215–225. https://doi.org/10.1016/j.jcis.2019.10.035.

Lotha, T.N., Sorhie, V., Bharali, P. and Jamir, L., 2024. Advancement in Sustainable Wastewater Treatment: A Multifaceted Approach to Textile Dye Removal through Physical, Biological and Chemical Techniques. *ChemistrySelect*, 11(9), p.e202304093. https://doi.org/10.1002/slct.202304093.

Lou, Z., Wang, Q., Kara, U.I., Mamtani, R.S., Zhou, X., Bian, H., Yang, Z., Li, Y., Lv, H., Adera, S. and Wang, X., 2022. Biomass-derived carbon heterostructures enable environmentally adaptive wideband electromagnetic wave absorbers. *Nano-Micro Letters*, 14(1), pp.1–16. https://doi.org/10.1007/s40820-021-00750-z.

Luo, X., Song, X., Cao, Y., Song, L. and Bu, X., 2020. Investigation of calcium carbonate synthesized by steamed ammonia liquid waste without use of additives. *RSC Advances*, 10(13), pp.7976–7986. https://doi.org/10.1039/c9ra10460g.

Manjuladevi, M. and Sri, O.M., 2017. Heavy metals removal from industrial wastewater by nano adsorbent prepared from *Cucumis melopeel* activated carbon. *Journal of Nanomedicine Research*, 5(1), pp.1–4. https://doi.org/10.15406/jnmr.2017.05.00102.

Mondal, N.K. and Basu, S., 2019. Potentiality of waste human hair towards removal of chromium(VI) from solution: kinetic and equilibrium studies. *Applied Water Science*, 9(3), pp.1–8. https://doi.org/10.1007/s13201-019-0929-5.

Mukherjee, A., Zimmerman, A.R. and Harris, W., 2011. Surface chemistry variations among a series of laboratory-produced biochars. *Geoderma*, 163(3–4), pp.247–255. https://doi.org/10.1016/j.geoderma.2011.04.021.

Muthukumaran, C., Sivakumar, V.M. and Thirumarimurugan, M., 2016. Adsorption isotherms and kinetic studies of crystal violet dye removal from aqueous solution using surfactant modified magnetic nanoadsorbent. *Journal of the Taiwan Institute of Chemical Engineers*, 63(6), pp.354–362. https://doi.org/10.1016/j.jtice.2016.03.034.

Muzarpar, M.S., Leman, A.M., Rahman, K.A., Shayfull, Z. and Irfan, A.R., 2020. Exploration sustainable base material for activated carbon production using agriculture waste as raw materials: a review. *IOP Conference Series: Materials Science and Engineering*, 864(1). https://doi.org/10.1088/1757-899X/864/1/012022.

Nejadshafiee, V. and Islami, M.R., 2019. Adsorption capacity of heavy metal ions using sultone-modified magnetic activated carbon as a bio-adsorbent. *Materials Science and Engineering: C*, 101(July), pp.42–52. https://doi.org/10.1016/j.msec.2019.03.081.

Park, J.E., Lee, G.B., Kim, H. and Hong, B.U., 2022. High surface area–activated carbon production from cow manure controlled by heat treatment conditions. *Processes*, 10(7), pp.1–13. https://doi.org/10.3390/pr10071282.

Parvin, S., Hussain, M.M., Akter, F. and Biswas, B.K., 2021. Removal of congo red by silver carp (hypophthalmichthys molitrix) fish bone powder: kinetics, equilibrium, and thermodynamic study. *Journal of Chemistry*, 2021. https://doi.org/10.1155/2021/9535644.

Pathak, H., 2023. Impact, adaptation, and mitigation of climate change in Indian agriculture. *Environmental Monitoring and Assessment*, 195(1), pp.1–22. https://doi.org/10.1007/s10661-022-10537-3.

Pongener, C., Bhomick, P.C., Supong, A., Baruah, M., Sinha, U.B. and Sinha, D., 2018. Adsorption of fluoride onto activated carbon synthesized from Manihot esculenta biomass - Equilibrium, kinetic and thermodynamic studies. *Journal of Environmental Chemical Engineering*, 6(2), pp.2382–2389. https://doi.org/10.1016/j.jece.2018.02.045.

Prajapati, A.K. and Mondal, M.K., 2020. Comprehensive kinetic and mass transfer modeling for methylene blue dye adsorption onto CuO nanoparticles loaded on nanoporous activated carbon prepared from waste coconut shell. *Journal of Molecular Liquids*, 307(3), p.112949. https://doi.org/10.1016/j.molliq.2020.112949.

Rajhans, G., Sen, S.K., Barik, A. and Raut, S., 2020. Elucidation of fungal dye-decolourizing peroxidase (DyP) and ligninolytic enzyme activities in decolourization and mineralization of azo dyes. *Journal of Applied Microbiology*, 129(6), pp.1633–1643. https://doi.org/10.1111/jam.14731.

Rajkumar, S., Murugesh, S., Sivasankar, V., Darchen, A., Msagati, T.A.M. and Chaabane, T., 2019. Low-cost fluoride adsorbents prepared from a renewable biowaste: Syntheses, characterization and modeling studies. *Arabian Journal of Chemistry*, 12(8), pp.3004–3017. https://doi.org/10.1016/j.arabjc.2015.06.028.

Rehman, R., Abbas, A., Murtaza, S., Mahmud, T., Waheed-Uz-Zaman, Salman, M. and Shafique, U., 2012. Comparative removal of Congo Red dye from water by adsorption on *Grewia asiatica* leaves, Raphanus sativus peels and activated charcoal. *Journal of the Chemical Society of Pakistan*, 34(1), pp.112–119.

Sh, H., El-taweel, R.M., Alrefaey, K.A., Labena, A., Fahim, I.S., Said, L.A. and Radwan, A.G., 2024. Enhanced removal of crystal violet using raw fava bean peels, its chemically activated carbon compared with commercial activated carbon. *Case Studies in Chemical and Environmental Engineering*, 9(10), p.100534. https://doi.org/10.1016/j.cscee.2023.100534.

Shen, F., Liu, J., Zhang, Z., Dong, Y. and Gu, C., 2018. Density functional study of hydrogen sulfide adsorption mechanism on activated carbon. *Fuel Processing Technology*, 171(9), pp.258–264. https://doi.org/10.1016/j.fuproc.2017.11.026.

Shukla, S.K., Al Mushaiqri, N.R.S., Al Subhi, H.M., Yoo, K. and Al Sadeq, H., 2020. Low-cost activated carbon production from organic waste and its utilization for wastewater treatment. *Applied Water Science*, 10(2), pp.1–9. https://doi.org/10.1007/s13201-020-1145-z.

Srinivas Kini, M., Balakrishna Prabhu, K., Gundecha, A. and Devika, U., 2017. Statistical analysis of Congo red dye removal using sawdust activated carbon. *International Journal of Applied Engineering Research*, 12(19), pp.8788–8804.

Standard, A.S.T.M., 1999. Standard test methods for moisture in activated carbon. *Philadelphia, PA: ASTM Committee on Standards*.

Stevens, M.G.F. and Batlokwa, B.S., 2017. Environmentally friendly and cheap removal of lead (ii) and zinc (ii) from wastewater with fish scales

waste remains. *International Journal of Chemistry*, 9(4), p.22. https://doi.org/10.5539/ijc.v9n4p22.

Sundararaman, S., Kumar, P.S., Deivasigamani, P., Jagadeesan, A.K., Devaerakkam, M., Al-Hashimi, A. and Choi, D., 2021. Assessing the plant phytoremediation efficacy for azolla filiculoides in the treatment of textile effluent and redemption of Congo red dye onto azolla biomass. *Sustainability*, 13(17). https://doi.org/10.3390/su13179588.

Supong, A., Bhomick, P.C., Baruah, M., Pongener, C., Sinha, U.B. and Sinha, D., 2019a. Adsorptive removal of Bisphenol A by biomass activated carbon and insights into the adsorption mechanism through density functional theory calculations. *Sustainable Chemistry and Pharmacy*, 13(April), p.100159. https://doi.org/10.1016/j.scp.2019.100159.

Supong, A., Bhomick, P.C., Karmaker, R., Ezung, S.L., Jamir, L., Sinha, U.B. and Sinha, D., 2020. Experimental and theoretical insight into the adsorption of phenol and 2,4-dinitrophenol onto Tithonia diversifolia activated carbon. *Applied Surface Science*, 529(06), p.147046. https://doi.org/10.1016/j.apsusc.2020.147046.

Supong, A., Bhomick, P.C., Sinha, U.B. and Sinha, D., 2019b. A combined experimental and theoretical investigation of the adsorption of 4-Nitrophenol on activated biocarbon using DFT method. *Korean Journal of Chemical Engineering*, 36(12), pp.2023–2034. https://doi.org/10.1007/s11814-019-0382-z.

Supong, A., Sinha, U.B. and Sinha, D., 2022. Density functional theory calculations of the effect of oxygenated functionals on activated carbon towards cresol adsorption. *Surfaces*, 5(2), pp.280–289. https://doi.org/10.3390/surfaces5020020.

Toor, M. and Jin, B., 2012. Adsorption characteristics, isotherm, kinetics, and diffusion of modified natural bentonite for removing diazo dye. *Chemical Engineering Journal*, 187, pp.79–88. https://doi.org/10.1016/j.cej.2012.01.089.

Torres, F.G., Troncoso, O.P., Nakamatsu, J., Grande, C.J. and Gómez, C.M., 2008. Characterization of the nanocomposite laminate structure occurring in fish scales from Arapaima Gigas. *Materials Science and Engineering: C*, 28(8), pp.1276–1283. https://doi.org/10.1016/j.msec.2007.12.001.

Ukanwa, K.S., Patchigolla, K., Sakrabani, R., Anthony, E. and Mandavgane, S., 2019. A review of chemicals to produce activated carbon from agricultural waste biomass. *Sustainability*, 11(22), pp.1–35. https://doi.org/10.3390/su11226204.

Van Tran, T., Bui, Q.T.P., Nguyen, T.D., Le, N.T.H. and Bach, L.G., 2017. A comparative study on the removal efficiency of metal ions (Cu^{2+}, Ni^{2+}, and Pb^{2+}) using sugarcane bagasse-derived $ZnCl_2$-activated carbon by the response surface methodology. *Adsorption Science & Technology*, 35(1–2), pp.72–85. https://doi.org/10.1177/0263617416669152.

Wang, X., Zhang, A., Chen, M., Seliem, M.K., Mobarak, M., Diao, Z. and Li, Z., 2023. Adsorption of azo dyes and Naproxen by few-layer MXene immobilized with dialdehyde starch nanoparticles: Adsorption properties and statistical physics modeling. *Chemical Engineering Journal*, 473(10), p.145385.

Yazid, H., Achour, Y., Kassimi, A.E., Nadir, I., Himri, M.E., Laamari, M.R. and Haddad, M.E., 2021. Removal of congo red from aqueous solution using cuttlefish bone powder. *Physical Chemistry Research*, 9(4), pp.565–577. https://doi.org/10.22036/pcr.2021.278943.1901.

Yin, H., Qiu, P., Qian, Y., Kong, Z., Zheng, X., Tang, X.Z. and Guo, H., 2019. Textile wastewater treatment for water reuse: A case study. *Processes*, 7(1), pp.1–21. https://doi.org/10.3390/pr7010034.

Zhang, S., Zheng, M., Lin, Z., Li, N., Liu, Y., Zhao, B., Pang, H., Cao, J., He, P. and Shi, Y., 2014. Activated carbon with ultrahigh specific surface area synthesized from natural plant material for lithium-sulfur batteries. *Journal of Materials Chemistry A*, 2(38), pp.15889–15896. https://doi.org/10.1039/c4ta03503h.

Zhou, Y., Ge, L., Fan, N. and Xia, M., 2018. Adsorption of Congo red from aqueous solution onto shrimp shell powder. *Adsorption Science & Technology*, 36(5–6), pp.1310–1330. https://doi.org/10.1177/0263617418768945.

Zhu, K., Gong, X., He, D., Li, B., Ji, D., Li, P., Peng, Z. and Luo, Y., 2013. Adsorption of Ponceau 4R from aqueous solutions using alkali boiled Tilapia fish scales. *RSC Advances*, 3(47), pp.25221–25230. https://doi.org/10.1039/c3ra43817a.

ORCID DETAILS OF THE AUTHORS

Vevosa Nakro: https://orcid.org/0000-0002-0487-0148
Ketiyala Ao: https://orcid.org/0009-0001-2330-2963
Tsenbeni N Lotha: https://orcid.org/0000-0002-5337-7851
Imkongyanger Ao: https://orcid.org/0009-0002-7116-6756
Lemzila Rudithongru: https://orcid.org/0000-0003-3983-9279
Chubaakum Pongener: https://orcid.org/0000-0002-7708-7162
Merangmenla Aier: https://orcid.org/0000-0002-3672-3126
Aola Supong: https://orcid.org/0000-0003-4367-6775
Latonglila Jamir: https://orcid.org/0000-0003-4039-9426